A Global and a Segmented Plane Scatter Calibration: Improving the Quantitative Accuracy of Frames with High Random Fraction and/or Low Number of Counts in Dynamic High Resolution PET Brain Imaging

Ju-Chieh (Kevin) Cheng, Arman Rahmim, *Member, IEEE,* Stephan Blinder, and Vesna Sossi, *Member, IEEE*

***Abstract*– We describe a scatter calibration technique which compensates for the noisy scaling across the planes and the over-scaling bias in the scatter estimation for scans with high random fraction and/or low number of counts, a situation often encountered in dynamic imaging on scanners with a large number of lines-of-response (LOR) such as the High Resolution Research Tomograph (HRRT). This calibration technique is based on the observations that the scatter fraction is relatively constant as a function of time. i.e. the amount of scatter is proportional to the number of true counts within each dynamic frame with the same proportionality constant. In this work, we first demonstrate the bias in the scatter scaling using the Single Scatter Simulation (SSS) for frames with high random fractions and low number of counts using a phantom study acquired with the HRRT, and we then present two new approaches to scatter correction scaling: a global scatter calibration (GSC) and a segmented plane-based scatter calibration (SPSC) technique. The improvement achieved with GSC and SPSC was examined by comparing the global scatter fraction for the aforementioned frames between the scatter estimates obtained with and without the calibration. The scatter fraction and the scatter sinogram for each segment were also compared between GSC and SPSC method. A significant bias in scatter fraction was found for frames which contain a random fraction higher than 40% with a number of counts less than 10M. For example, a scatter fraction of as high as 270% was obtained from a frame with 90% random fraction and 2M counts, whereas the correct scatter fraction was approximately 40%. A much more consistent global scatter fraction of about 40% was obtained by both GSC and SPSC as compared to the conventional method, and a smoother scatter estimation was achieved by applying SPSC. The potential improvement in the voxel time activity curve (TAC) by applying the calibration is also shown for a cylindrical phantom, non-human primate, and human brain studies.**

This work was supported by the Canadian Institute of Health Research, the TRIUMF Life Science grant, and the Michael Smith Foundation for Health Research scholarship (V. Sossi).

J.-C. Cheng and V. Sossi are with the Department of Physics and Astronomy, University of British Columbia, Vancouver, BC V6T 1Z1 (e-mail jcheng@phas.ubc.ca, vesna@phas.ubc.ca).

A. Rahmim is with the Department of Radiology, Johns Hopkins University School of Medicine, Baltimore, MD 21205 (e-mail arahmim1@jhmi.edu).

S. Blinder is with the Pacific Parkinson's Research Centre, Vancouver, BC, V6T 1Z1 (e-mail blinder@phas.ubc.ca).

I. INTRODUCTION

SCATTER correction is one of the biggest challenges in PET imaging since the reconstructed images are not quantitative when the measured true coincidences are contaminated with scattered events. The widely used scatter estimation process for 3D PET generally consists of two parts: one is to obtain the spatial scatter distribution within the object, and the other is to scale the magnitude of that distribution to account for scatter originated from outside the field of view (FOV) and to make it commensurate to the measured true coincidences. The scaling process is generally done by fitting the tails of the estimated scatter distribution to the tails of the measured true coincidences [1]. The true coincidences are obtained by subtracting the measured random (delayed coincident) events from the measured prompts. Therefore, when the random fraction is high and/or the number of acquired counts is low, the estimate of true coincidences for many sinogram bins or lines-of-response (LORs) may result into negative numbers especially for high resolution scanners which have hundreds of millions of LORs. Typically, in order to prevent the negative scaling in the scatter, a positivity-constraint is applied. However, the positivity-constraint is prone to introducing an overestimation bias into the scatter estimate which, in turn, leads to an underestimated emission image. Dynamic scanning with short lived radiotracers is particularly susceptible to such biases for the early frames which tend to be short and acquired at high count rates.

In typical dynamic imaging, the scatter events are generally estimated on a frame-by-frame basis. The justification for this approach is that the tracer distribution changes as a function of time, and therefore the scatter distribution changes accordingly. Given the often highly variable number of events per frame typical of dynamic scanning and variable count rates at which the acquisition is performed, the number of counts in each frame might not always be sufficient to produce an accurate scatter scaling across the plane. In this work, we first demonstrate the bias in the scatter scaling using the Single Scatter Simulation (SSS) [1] [2] for frames with high random fractions and low number of counts (corresponding to typical dynamic human and non-human primate studies) using a phantom study acquired with the High Resolution Research Tomograph (HRRT), and we then present two new approaches to scatter correction scaling: a global scatter calibration (GSC)

and a segmented plane scatter calibration (SPSC) technique which compensate the aforementioned bias.

II. A GLOBAL (GSC) AND A SEGMENTED PLANE SCATTER CALIBRATION (SPSC) TECHNIQUE

This technique is based on two related observations:

- Both scattered and unscattered true events are proportional to the radioactivity thus making the temporal scatter fraction approximately constant as long as (i) the anatomical structure of the object does not change over time, (ii) it has a relatively uniform density distribution (e.g. head) and (iii) there is no drastic change in the radioactivity distribution.
- The amount (magnitude) of scatter in each dynamic frame is proportional to the number of true counts in the frame (at least in the global and segment level as will be discussed shortly).

A reference scatter estimate which is free from the overestimation bias (i.e. obtained from a frame with a low random fraction and a high number of counts) is required to perform this calibration on the biased scatter estimate. For example, in dynamic studies the scatter estimated from a summed frame can be used as the reference. Consequently, by summing over all the scatter counts in the reference scatter estimate and scaling the sum according to the number of true counts in the frame whose scatter estimate needs to be calibrated, one can obtain the expected or calibrated total scatter counts in the potentially biased frame. The calibration factor is obtained by dividing the expected or calibrated total scatter counts by the total scatter counts from the biased scatter estimate as shown in Eq. (1).

$$S_c^G = F_{sc}^G * S_b^G,\ F_{sc}^G = \left(\frac{c_{tb}}{c_{tr}}\right)^G \left(\frac{c_{sr}}{c_{sb}}\right)^G \text{ for GSC} \qquad (1)$$

where S_c is the scatter estimate after calibration, S_b is the (biased) scatter estimate from the original frame, F_{sc} is the scatter calibration factor (either on a frame, segment, or plane basis as will be discussed shortly), C_{sr} is the number of scatter counts in the reference frame, C_{sb} is the number of scatter counts in the original (biased) frame, C_{tb} is the number of true counts in the original (biased) frame, C_{tr} is the number of true counts in the reference frame, and the superscript G represents the quantity in the global level.

This calibration can be done as a global correction factor for the scatter (i.e. preserve the original calculated 'frame spatial scatter distribution' and correct for the overall scaling: GSC); it can also be applied to each segment of the scatter sinogram or even on a plane-by-plane basis (i.e. preserve the original calculated 'plane spatial scatter distribution' and correct for the scaling for each plane: SPSC). However, the difficulty for this technique to be applied on a plane-by-plane basis is to obtain a reasonable ratio of the trues (i.e. C_{tb}/C_{tr}) since the total number of true counts for each plane in a frame with a low number of counts may be statistically too uncertain to obtain a reliable ratio. Moreover, the scaling according to the trues ratio in the plane level can only be done when the temporal plane scatter fraction is constant which is not quite true since the spatial scatter distribution is very smooth and is not very sensitive to the tracer distribution. As a result, dividing the slowly-changing scatter by the temporally fast-varying trues for each plane (i.e. temporal plane scatter fraction) will not be very constant temporally. The trick to make the calibration work in the plane level is either i) using the global trues ratio or ii) using the trues ratio obtained from each segment since the temporal global and segment scatter fraction is much more constant in the dynamic scans (though an additional assumption that the one dimensional axial scatter distribution is smooth and approximately constant over time needs to be imposed). However, scaling the scatter according to the global trues ratio preserves the biased pattern in the segment scatter fraction as will be discussed in the result section; as a result, scaling according to the trues ratio obtained from the segment level was determined to be the more accurate method (SPSC) as shown in Eq. (2).

$$S_c^P = F_{sc}^P * S_b^P,\ F_{sc}^P = \left(\frac{c_{tb}}{c_{tr}}\right)^S \left(\frac{c_{sr}}{c_{sb}}\right)^P \text{ for SPSC} \qquad (2)$$

where the superscript P represents the quantity in the plane level, and the superscript S represents the quantity in the segment level.

III. METHODS

Tomograph: Data were acquired on the second generation of the High Resolution Research Tomography (HRRT) [3, 4]. This HRRT scanner has an octagonal detector ring design, with detector heads consisting of a double 10 mm layer of LSO/LYSO for a total of 119,808 detector crystals.

Phantom study: A 20 cm long, 20 cm diameter cylindrical phantom was used. The phantom was filled uniformly with an initial ^{11}C radioactivity concentration of 60.9 kBq/ml. Data were grouped into sets of frames with similar numbers of counts for various random fractions to evaluate the accuracy of the scatter fraction for the conventional (i.e. without any scatter calibration), GSC, and SPSC scatter estimation; 3 frames with ~2M counts, 3 frames with ~5M counts, 3 frames with ~10M counts, and 1 frame with ~50M counts (the summed frame) for random fractions of 20%, 40%, 60%, and 75% (i.e. 10 frames for each random fraction). An additional frame with ~2M counts for 90% random fraction was also examined (no other number of counts would correspond to a 90% random fraction in this study). These numbers of counts and random fractions were chosen since they are fairly representative of the number of counts encountered in human and non-human primate receptor imaging. The count rate for these frames was at least 500 times higher than the intrinsic LSO true coincidence rate (intrinsic LSO true coincidence rate is about 100 cps) in order to exclude the effect of the intrinsic LSO background contribution to the scatter fraction. A frame with 20% random fraction and 320M counts was used as the reference for the GSC and SPSC methods.

1) Scatter fraction (SF) comparisons (Fig. 1, 2, 3): The scatter estimates were computed in span 3 for each frame with the conventional, GSC, and SPSC methods, and the global scatter fractions for the aforementioned frames were calculated and plotted against random fraction for different number of counts. The scatter fraction for each segment was calculated for the frame with 90% random fraction and 2M counts for GSC, SPSC, and also for the reference frame. The segment scatter fraction (i.e. scatter fraction averages over sinograms belonging to the same segment or same axial angle) was then plotted for each segment.

2) Scatter sinogram comparisons (Fig. 4): The scatter sinograms obtained from the frame with 90% random fraction and 2M counts using the conventional, GSC, and SPSC methods and that obtained from the reference frame were compared visually.

3) Voxel ratio comparisons (Fig. 5, 6): The true emission images were reconstructed for frames which contain 10% and 40% random fraction and with prompts range from 2M to 50M using the conventional and SPSC methods. The voxel ratios between images reconstructed using the conventional scatter estimate and those reconstructed using SPSC method were plotted as a function of prompts.

Non-human primate study (Fig. 9): The regular dynamic framing scheme was performed to check the influence of SPSC method on the voxel TAC. The random fraction of this study ranges from 74% to 14% with the prompts range from 6M to 71M. (note that the first frame contains a random fraction of 74% and 21M counts)

Human studies: The first frame of a human study which contains a 95% random fraction and 2.6M counts (the worst case encountered so far) was used to examine the effect of the SPSC method. The segment zero scatter sinograms and the axial scatter profiles for the conventional method with and without the positivity-constraint are also compared with those obtained by SPSC (Fig. 7, 8).

Another human study with the proper motion information (~ 1mm of patient motion) was used to check the influence of SPSC on the voxel TAC (Fig. 10). The random fraction of this study ranges from 74% to 9% with the prompts range from 3.4M to 62M. (note that the first frame contains a random fraction of 74% and 3.4M counts)

IV. Results

Phantom study: A scatter fraction of 39.4% was obtained from the reference frame for the phantom study, and the over-scaling in the conventional scatter estimates is demonstrated in Fig. 1. As expected, the scatter fraction gets closer and closer to the reference value as the number of counts increases and as the random fraction decreases since it is less likely to get negative true counts. The worst case here shows a biased scatter fraction as high as 270% obtained from a frame with 90% random fraction and 2M counts. As a result, the true emission images are globally underestimated due to the over-subtraction of the scatter.

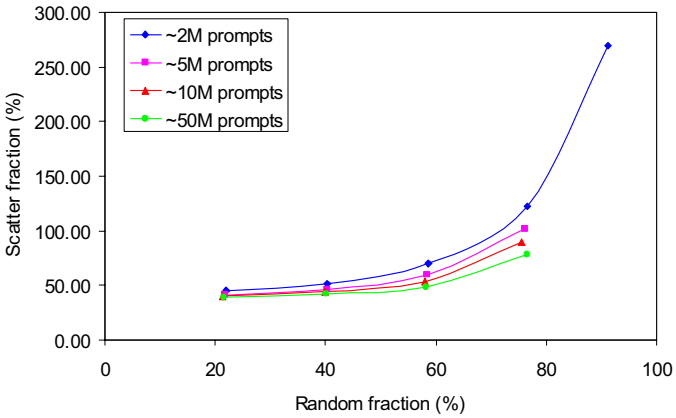

Fig. 1: The global scatter fraction as a function of random fraction for various numbers of counts using the conventional method

The improvement achieved in the global scatter fraction using the GSC and SPSC methods is shown in Fig. 2; a very consistent global scatter fraction was obtained for both methods.

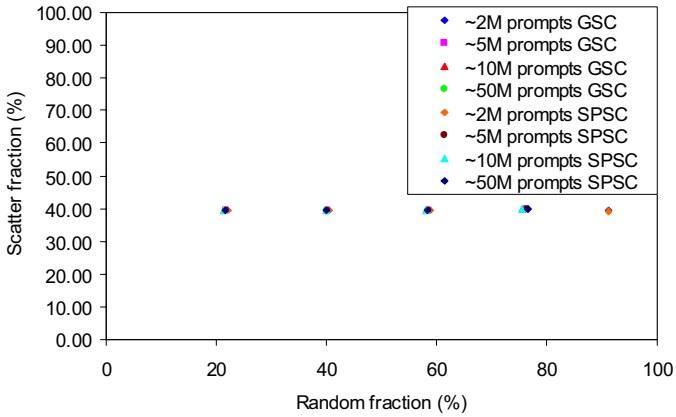

Fig. 2: The global scatter fraction as a function of random fraction after applying GSC and SPSC

As shown in Fig. 3, a larger variation in the segment scatter fraction was obtained with the GSC as compared to the reference and SPSC since it only corrects for the global magnitude of the scatter (scaling the scatter according to the global trues ratio only ensures a consistent global scatter fraction), whereas SPSC corrects the scaling for each plane and produces a 'smoother' estimate as depicted in Fig. 4d (scaling according to the segment trues ratio ensures both consistent global and segment scatter fractions and note the only difference between Fig. 4b and 4c is just the scale). One can also observe the noisy scaling across the plane due to the statistical variation of counts in each plane.

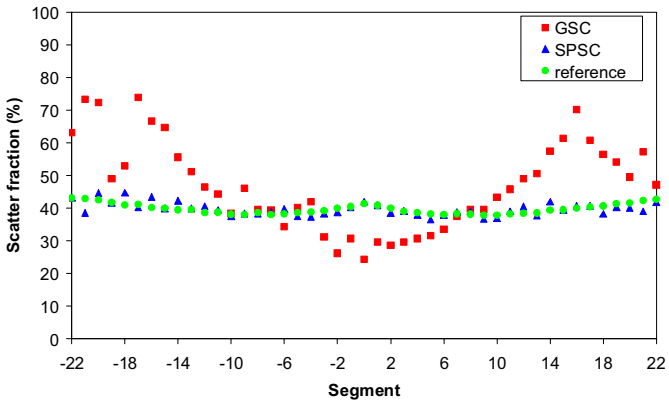

Fig. 3: The segment scatter fraction for the frame calibrated with GSC, SPSC, and for the reference frame

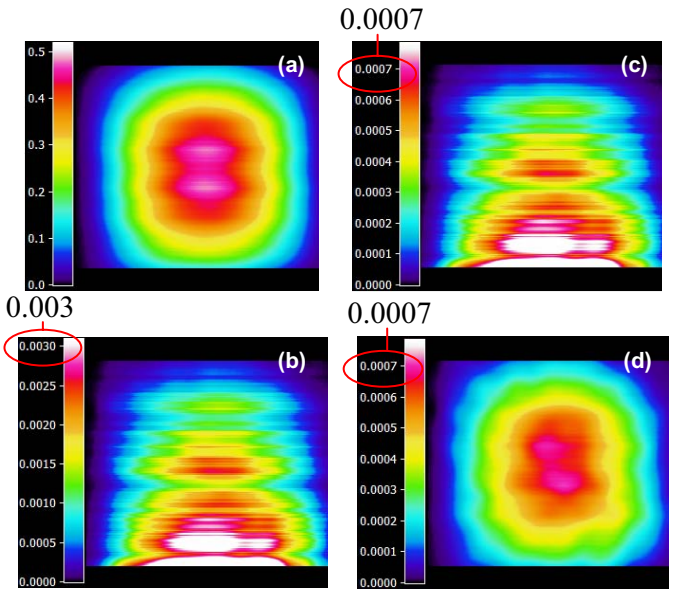

Fig. 4: The z-r view of the segment zero scatter sinogram which shows all 207 planes (a) for the reference, (b) for the bias frame, (c) after calibrating with GSC and (d) SPSC

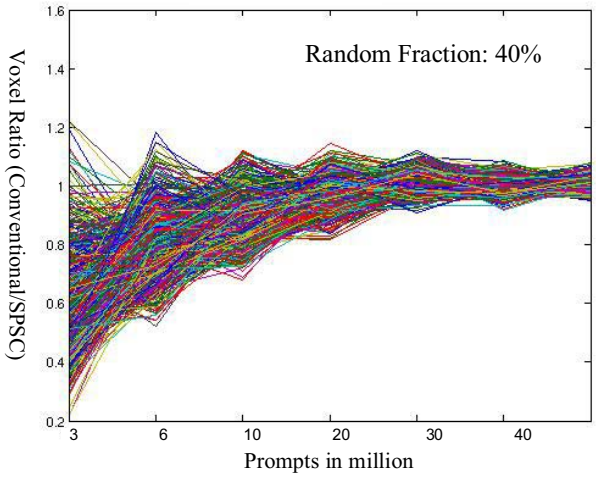

Fig. 5: Image voxel ratio between data reconstructed with the conventional and those reconstructed with SPSC method as a function of number of measured prompts for a random fraction of 40% for the phantom study

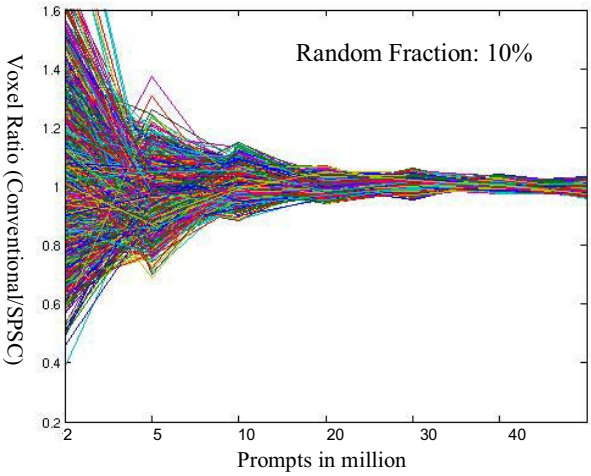

Fig. 6: Image voxel ratio between data reconstructed with the conventional and those reconstructed with SPSC method as a function of number of measured prompts for a random fraction of 10% for the phantom study

The voxel ratio comparison for a random fraction of 40% demonstrates the influence of both the positivity-constraint and the noisy scatter scaling as shown in Fig. 5. The voxel ratio comparison for a random fraction of 10% shows the potential improvement which can be achieved by smoothing the scatter scaling across the planes (SPSC) as depicted in Fig. 6. In addition, the bias decreases as the prompts increase, and more prompts are needed to reduce the bias for a higher random fraction.

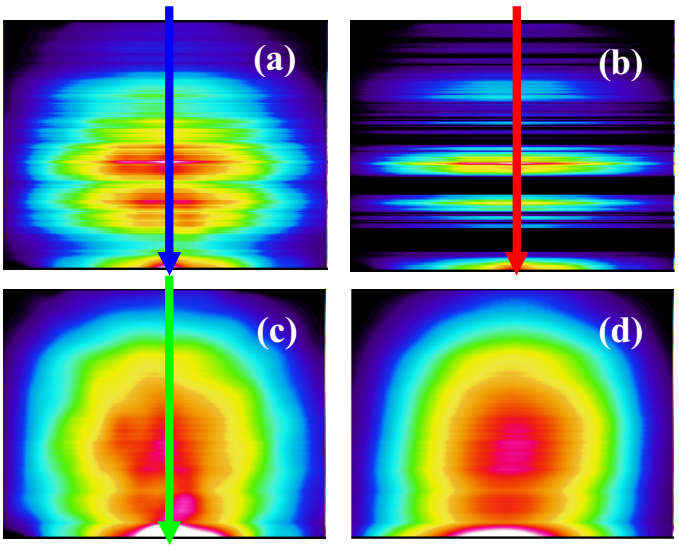

Fig. 7: The z-r view of the segment zero scatter sinogram (a) with the positivity-constraint, (b) without the constraint, (c) calibrated with SPSC, and (d) the reference for the first dynamic frame of the human study

Human and non-human primate studies: Fig. 7 shows the z-r view of the segment zero scatter sinogram for the first frame of the human study which contains a random fraction of 95% and 2.6M counts. The sinograms obtained with both conventional methods (with and without the positivity-constraint) show very noisy scaling across the planes. The sinogram calibrated with SPSC shows a much smoother scaling across the planes with a global scatter fraction of

~43%. The axial scatter profile is shown in Fig. 8. The overestimation bias can be easily observed for the conventional method with the positivity-constraint (the global scatter fraction is ~350% and clearly there are very few counts left in the emission image after subtracting too much scatter), and even though the global scatter fraction for the conventional method without the constraint is ~47% which is much more accurate than the one with the constraint, the negative and noisy scaling still makes it suboptimal as demonstrated in Fig. 7b and 8. The scatter profile obtained with SPSC appears to be closer to the expected scatter distribution.

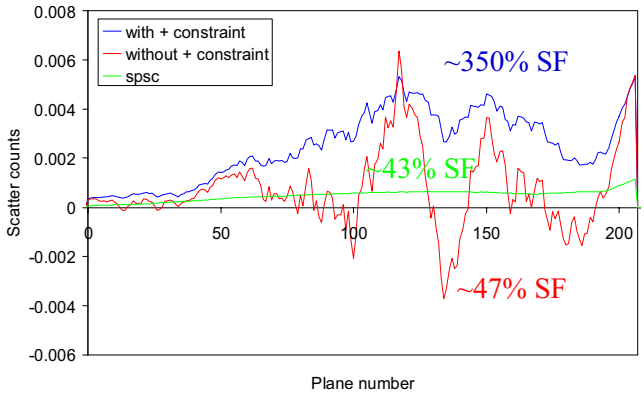

Fig. 8: The profiles across the planes for Figure 7 (a), (b), and (c) together with the corresponding global scatter fraction (SF)

Fig. 9 shows the voxel TAC ratio (conventional/SPSC) comparison for the non-human primate study. As expected, the first few frames show a bigger difference due to the initial high random fraction, and the last few frames show an increasing difference due to the decreasing number of counts as a consequence of radioactivity decay. Note that the difference in the first frame is within ~ ±10% since the frame contains more than 20M counts, and the difference starts to increase when the number of counts within a frame is less than ~13M counts.

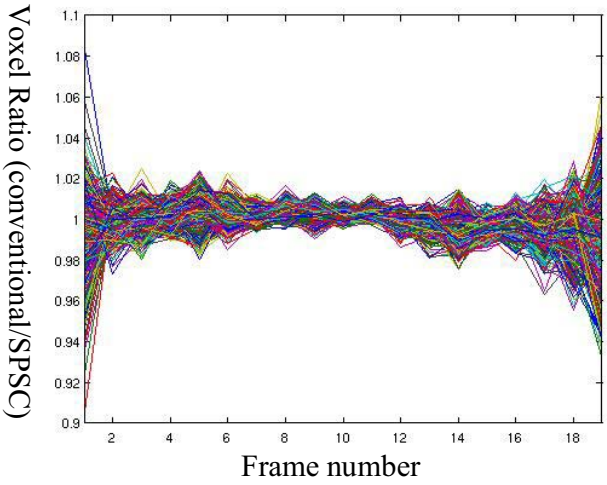

Fig. 9: Image voxel TAC ratio between data reconstructed with the conventional and those reconstructed with SPSC method for the non-human primate study

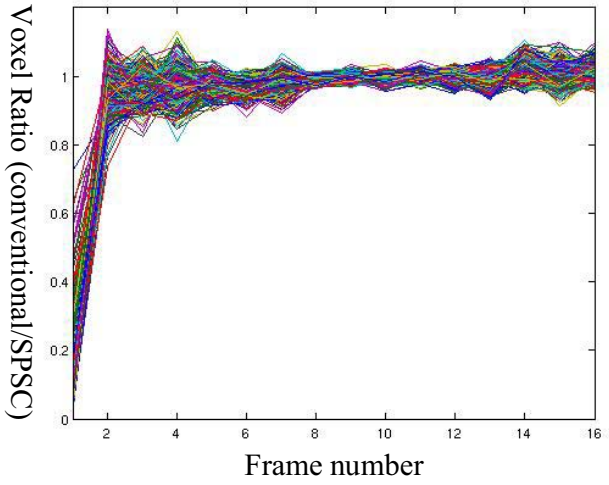

Fig. 10: Image voxel TAC ratio between data reconstructed with the conventional and those reconstructed with SPSC method for the human study

Fig. 10 shows the same comparison for the human study. Here all frames contain fewer counts compared to the non-human primate study (e.g. the first frame of this human study contains only 3M counts, whereas the non-human primate one contains more than 20M counts). As a result, the scatter in the first frame of the human study is largely influenced by the positivity-constraint, and the voxel ratio shows a more than 50% difference between the image intensities (voxel values) obtained with the two scatter estimates. A similar trend as the non-human primate study was observed (i.e. bigger difference at the 'head' and 'tail', and smaller difference at the 'center').

V. Conclusion and Future Work

We have developed a calibration technique which compensates for the overestimation bias and the noisy scaling in the scatter estimates for high resolution dynamic PET studies. Currently we are investigating in further detail if the assumptions used for the calibration introduce any significant bias in the reconstructed images. In addition, this calibration can also be incorporated into the practical scatter approximation technique [5] to further improve the accuracy for frames with larger change in the tracer distribution (typically frames with high random fraction and low number of counts).

Acknowledgment

The authors would like to thank Dr. Doris Doudet for providing the non-human primate data.

References

[1] C. C. Watson, "New, Faster, Image-Based Scatter Correction for 3D PET," *IEEE Trans. Nucl. Sci.* , vol. 47, pp. 1587-1594, 2000.

[2] C. C. Watson, M. E. Casey, C. Michel and B. Bendriem, "Advances in Scatter Correction for 3D PET/CT," *IEEE Med. Imaging Conf. Rec.* 4: 2195-9, 2004.

[3] de Jong H, van Velden FH, Kloet RW, Performance evaluation of the ECAT HRRT: an LSO-LYSO double layer high resolution, high sensitivity scanner. Phys Med Biol. 52(5):1505-26, 2007.

[4] V. Sossi, H. W.A.M. de Jong, W. C. Barker, P. Bloomfield, Z. Burbar, M-L Camborde, C. Comtat, L. A. Eriksson, S. Houle, D. Keator, C. Kn¨oß, R. Krais, A. A. Lammertsma, A. Rahmim, M. Sibomana, M. Ter¨as, C. J. Thompson, R. Tr´ebossen, J. Votaw, M. Walker, K. Wienhard and D. F. Wong," The Second Generation HRRT - a Multi-Centre Scanner Performance Investigation," *IEEE Med. Imag. Conf. Rec.,* 2005.

[5] J.-C. K. Cheng, A. Rahmim, S. Blinder, M-L Camborde, K. Raywood, and V. Sossi, "A scatter-corrected list-mode reconstruction and a practical scatter/random approximation technique for dynamic PET imaging," *Phys. Med. Biol.* 52: 2089-2106, 2007.